ALEPH 94-085
PHYSIC 94-073
V. Bertin et al.
08.06.1994

MEASUREMENT OF THE QUARK-TO-PHOTON FRAGMENTATION FUNCTION AT LEP

V.Bertin[1], M.G.Smith[2], A.S.Thompson[2], J.C.Thompson[1]

[1] *Rutherford Appleton Laboratory*
[2] *University of Glasgow*

Abstract

Earlier measurements at LEP of isolated hard photons in hadronic Z^0 decays attributed to radiation from primary quark pairs, have been extended in the ALEPH experiment to include their production *inside* hadron jets. Events are selected where all particles combine "democratically" to form hadron jets, one of which contains a photon with a fractional energy $z \geq 0.7$. After the statistical subtraction of events arising from non-prompt photons, the quark-to-photon fragmentation function, $D(z)$, is extracted directly from the measured prompt production rate. Taking into account the perturbative contributions to $D(z)$ obtained in an $\mathcal{O}(\alpha\alpha_S)$ $\overline{MS}$ renormalisation scheme enables the unknown non-perturbative component of $D(z)$ to be determined at high z. This measurement provides a better description of quark bremmstrahlung than hitherto employed in high energy electron-positron and hadron-hadron collisions.

1 Introduction

Several studies have been made of the production of hard isolated prompt photons accompanying hadronic decays of the Z at LEP [1]. Their origin has been attributed to final state radiation (FSR) emitted at an early stage in the QCD parton evolution process initiated from the primary quark-antiquark pair. The main thrust of this work has been to compare with QCD $\mathcal{O}(\alpha\alpha_S)$ calculations at the parton level, and to test the detailed predictions of the parton shower models, JETSET, HERWIG, and ARIADNE to gain some insight into the parton evolution mechanism. Many features of the data are well described by the QCD calculations giving confidence that the process is well measured and understood.

In all these analyses, the candidate photon was isolated from the hadronic debris in an event using a geometrical cone centred around its direction inside of which a minimal residue of accompanying hadronic energy was allowed. This procedure was considered necessary to reduce the non-prompt photon backgrounds from hadron decays. In the next step, the photon was removed from the event before jets were formed with the other particles using a clustering recombination algorithm. The consequence was that any particles associated with the photon were incorporated into the other jets. Finally, an event was retained only if the candidate photon remained apart from the jets in a second application of the clustering algorithm. The appropriate QCD calculations available [2, 3] employ different procedures to avoid the infra-red and collinear singularities in the cross section at the parton level. This leads to complications in matching the resulting phase space to that defined for the data [4].

It was pointed out [2] that a safer approach would be to apply a jet recombination scheme simultaneously to all particles in an event, including the photon. This "democratic" approach does give an unambiguous matching definition of phase space between experiment and theory for all event topologies and handles correctly those hadrons which are associated naturally with the photon. However, it introduces a significant non-perturbative contribution to the cross section which depends upon the amount of accompanying energy allowed in the "photon jet". At first sight, this would appear to prevent the accurate comparison of data with the QCD predictions employed earlier. However, this previously unknown parton fragmentation contribution can be measured, thus adding new information to the dynamics of quark radiation; and at the same time giving an improved comparison of all FSR data with the QCD calculations.

In this study, a sample of 1.17 million selected hadronic Z decay events are subdivided into 2-jet, 3-jet and $\geq$ 4-jet topologies using the DURHAM E0 algorithm with the resolution parameter, y_{cut}, varied between 0.001 and 0.33. Events are kept where at least one of the reconstructed hadron jets contains a photon ($E_\gamma > 5$ GeV) carrying at least 70% of the total energy of the jet. The fractional energy z_γ of such a photon within a jet is defined as:

$$z_\gamma = \frac{E_\gamma}{(E_\gamma + E_{had})}$$

where E_{had} is the energy of all accompanying hadrons in the "photon jet" found by the clustering algorithm. Thus, events with completely isolated photons appear at $z_\gamma = 1$. Currently, the measured z_γ range is limited to $0.7 < z_\gamma < 1.0$ by residual hadronic decay backgrounds which are large for the 2-jet sample, i.e. events with a single hadron-jet + "photon-jet" topology. These backgrounds are subtracted statistically according to Monte Carlo predictions after direct experimental confirmation that the principle components, namely the inclusive π^0 rates, are adequately simulated.

Recently, a massless QCD $\mathcal{O}(\alpha\alpha_S)$ calculation [5] which includes the non-perturbative photon fragmentation terms has shown that the 2-jet z_γ distribution measures directly the quark-to-photon fragmentation function, $D(z_\gamma)$, when the final state partons and photon are treated "democratically". It is assumed that the reconstructed hadron jets can be equated directly with the parton jets formed in this QCD calculation. In this calculation, the non-perturbative part of the $D(z_\gamma)$ function is described by a leading order (LO) evolution equation which can only be specified when the initial contribution at some given mass scale, μ_0, is known; this mass scale is expected to be near $\Lambda_{\overline{MS}}$. Universal fits to the 2-jet distributions between $0.7 < z_\gamma < 0.95$ are obtained at various values of y_{cut} showing that this

part of the $D(z_\gamma)$ function can be described by the above LO equation plus an additional term which describes its initial value when the evolution scale equals μ_0. The best fit indicates that this starting value is non-zero and independent of y_{cut}; a low value of μ_0 ($\sim$ 200 MeV) is preferred.

The same QCD $\mathcal{O}(\alpha\alpha_S)$ calculation predicts the perturbative isolated photon component at $z_\gamma = 1$ for 2, 3 and 4 jet event topologies. With a suitable choice of α_S, we show that the data, as a function of y_{cut}, are in good agreement provided that the smearing effects of the DURHAM particle clustering scheme are taken into account.

2 Selection of Events with Final State Photons

2.1 Hadronic events selection

The data sample is based on all the PERF and MAYB runs from 1990, 1991 and 1992. The hadronic Z decays are selected using the standard CLASS 16 algorithm requiring at least 5 "good" charged tracks measured in the TPC and the total energy calculated using all the "good" charged tracks $E_{ch} > 10\%\sqrt{s}$. This selects a total sample of 1 170 849 events (162 491 from 1990, 291 925 from 1991 and 716 433 from 1992), recorded at centre of mass energies between 88.25 and 94.25 GeV.

In order to remove the events where a major fraction of the hadronic decays have been lost in the beam pipe, the thrust axis of the event is computed using all the ENFLW particles, and the event is kept if $|\cos\theta_{thrust}| < 0.95$ where θ_{thrust} is the polar angle of the thrust axis with respect to the beam axis.

2.2 Selection of single photon clusters

This analysis has been performed on the MINI-DST version 8 and makes use in particular of the information recorded in the EGID bank containing the EBNEUT photons.

The photon selection starts from all the ENFLW photons (almost identical to the GAMPEK photons) with an energy greater than 5 GeV. The photon is then only considered if its energy has been measured in a fully efficient region of the calorimeter. The photon is thus rejected if it belongs to a PECO situated close to a crack or in the overlap region, or if its polar angle θ_γ satisfies $|\cos\theta_\gamma| > 0.95$.

The main background of the analysis is due to the energetic π^0 where the overlapping of the two photons coming from the π^0 is faking a single photon cluster. The most efficient way to reduce this background is to use the so-called BULOS moments analysis of the cluster available for the EGID photons. In order to use this information for the ENFLW photons, a unambiguous correspondence has first to be established between ENFLW and EGID photons. This is achieved by requiring that only one ENFLW photon and one EGID photon have been extracted from the original PECO cluster. This EGID photon selection is done by asking the "Nature" flag to be equal to 1. Note that the ENFLW photon is rejected if its corresponding PECO is linked with a charged track, since the EGID clusters are not available in this case. This selection of single photon PECO clusters is already very efficient in reducing the π^0 background in the case where the two photons from its decay are resolved by the GAMPEK or the EBNEUT algorithms.

Having selected a sample of single PECO-GAMPEK-EBNEUT photons, a cut on the major axis of the cluster, available as the "Estimator 6" in the EGID bank, can now be performed to reduce further the π^0 background. For single photon clusters, the distribution of this quantity has been found to be different if the cluster is situated in the barrel or the end-cap part of the calorimeter, as well as between real data and fully simulated Monte Carlo events. A renormalisation of this parameter has thus been performed leading to a Gaussian distribution centered at 0 with a width equal to 1, independent of the energy and of the polar angle of the photon. In the case of Monte Carlo events, the major axis distribution has been adjusted to reproduce the data (Fig 1). This renormalisation has been checked using samples of $e^+e^- \to e^+e^-\gamma$ and $e^+e^- \to \mu^+\mu^-\gamma$ real data and Monte Carlo events with a photon energy between 5 and 45 GeV.

The single photon is then kept if the major axis σ_L of his cluster satisfies $-3 < \sigma_L < 2$.

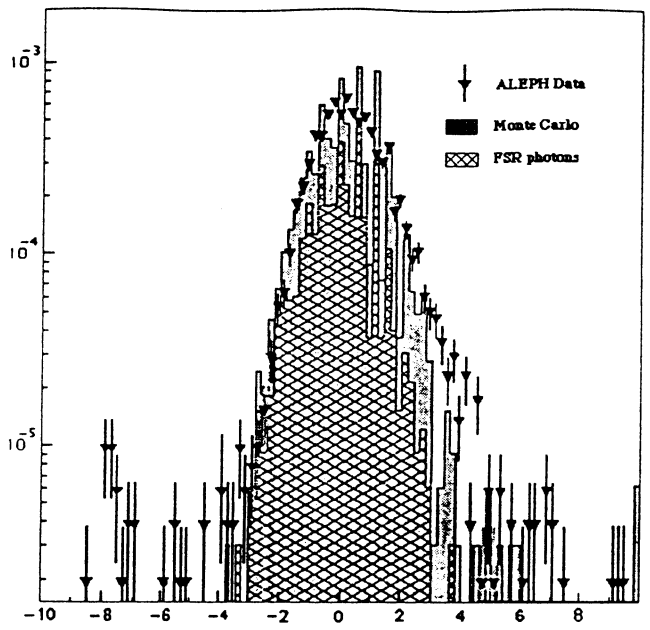

Figure 1: Distribution of the normalised major axis for single photon showers in real data and Monte Carlo.

The efficiency of this single photon selection has been measured using a sample of about 23 000 final state radiation (FSR) photons with an energy greater than 5 GeV coming from an equivalent sample of 2.7 million hadronic Z decays generated using ARIADNE3.3. The efficiency is 55% and is almost independent of the energy of the photon, with an inefficiency of 15% coming from photon conversions and the $|\cos\theta_\gamma|$ cut and an inefficiency of 20% due to the requirement of the PECO not to be in a crack or overlap region and not to be linked with a charged track. The single photon selection itself has an inefficiency of 10% and reduces the π^0 background by a factor of 3 and 2 at 20 GeV and 30 GeV respectively.

2.3 Selection of final state radiation events

For each event with at least one selected photon, jets are then constructed using all the energy flow objects of the event and treating the photon equally to all the other particles. The particle clustering is performed using the DURHAM E0 algorithm for 13 different y_{cut} values between 0.001 and 0.33. The jet resolution parameter y_{cut} is calculated for each event using the total observed energy flow. The event is kept if at least one selected photon has $z_\gamma > 0.7$ where z_γ is the fraction of the energy of the "photon jet" carried by the photon, as defined previously.

For each value of y_{cut}, the event sample is then divided into three categories corresponding to jet topologies of 2, 3 and ≥ 4 jets, where the number of jets includes the "photon jet". Fig 2 shows the observed z_γ distributions at $y_{cut} = 0.01$ subdivided by jet topology compared with the predictions of JETSET; the large background for 2-jet events is quite evident. For each topology, the z_γ distribution is divided into 6 equal bins between 0.7 and 1. In order to separate more clearly the large contribution coming from the hard photon component near $z_\gamma = 1$, the last bin is split into two parts: $0.95 < z_\gamma < 0.99$ and $0.99 < z_\gamma \leq 1$.

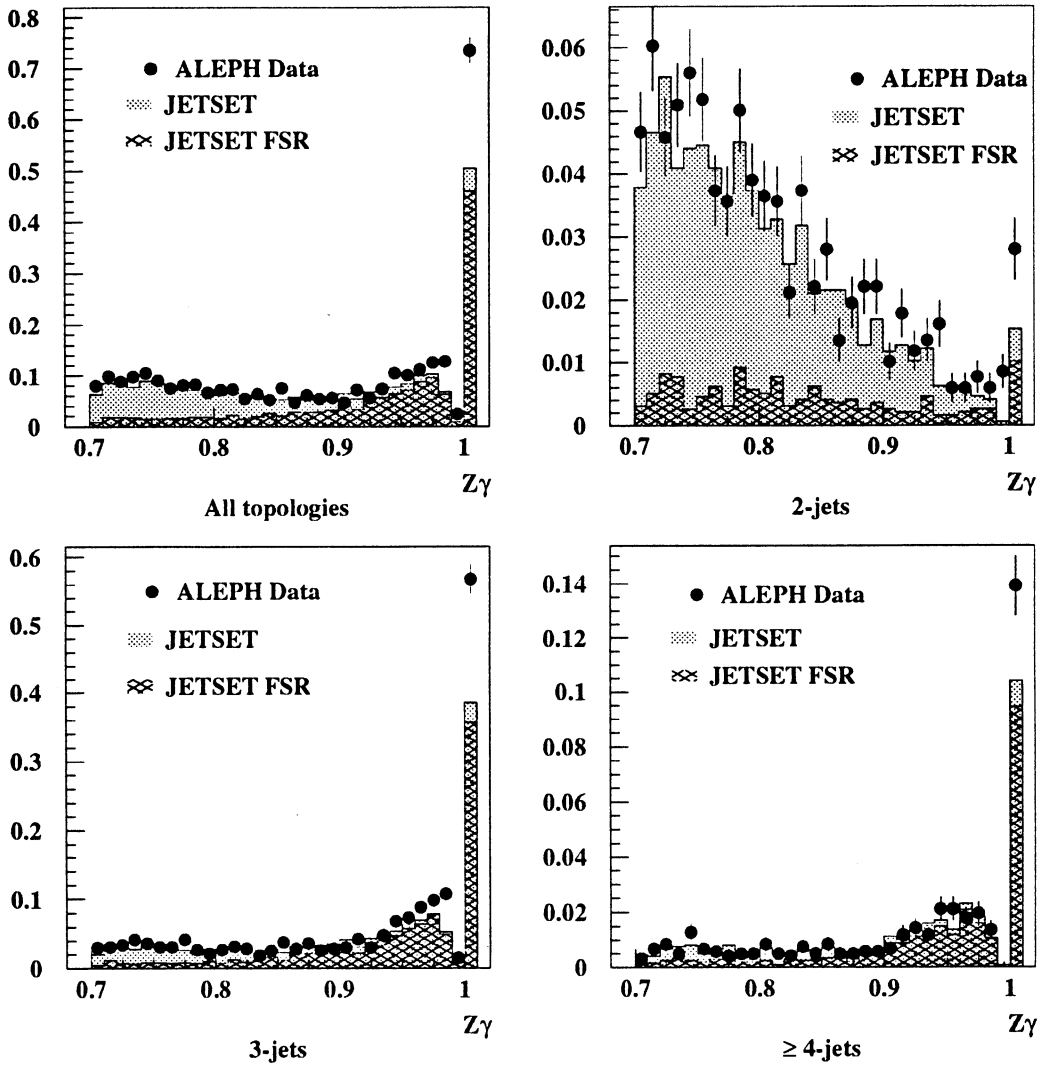

Figure 2: Observed z_γ distributions at $y_{cut} = 0.01$ in each topology before background substraction.

3 Background Subtraction and Systematic Errors

The irreducible background in the selected event sample arises mainly from the decays of neutral hadrons ($\pi^0, \eta, \ldots$) where the photon depositions spatially overlap in the electromagnetic calorimeter. Their contribution together with those from initial state radiation (ISR) and misidentified neutral hadrons is determined from a full simulation of JETSET events in the detector, and then subtracted statistically from the data bin-by-bin in z_γ for each value of y_{cut}. A small contribution from $Z \to \tau^+\tau^-$ decays which pass the hadronic event selection is also taken into account.

3.1 Initial State Radiation

The initial state radiation (ISR) background is estimated using a sample of 1.95 million hadronic events fully simulated in the detector. The ISR from the incoming leptons is generated by DYMU02 and the hadronic final state by JETSET7.3. Since ISR photons are mainly isolated, this background is very small for $z_\gamma < 0.90$ but becomes the dominant background for $z_\gamma > 0.99$. Its contribution to the total data sample is approximately independent of y_{cut} and event topology, being at the level of 5–10% for $z_\gamma > 0.99$, and about 1% for $z_\gamma < 0.90$. The systematic error in the ISR rate is assigned to be 5% [1].

3.2 Non-prompt Photons from Hadron Decays

For the 2-jets sample the background from overlapping photons which appear as single depositions in the ECAL dominates the measured signal when $z_\gamma < 0.9$. Hence, a good understanding of this background is essential to the extraction of the FSR signal. Its contribution is determined using the sample of 1.95 million simulated hadronic events described above. The purity of the FSR signal in the measured events, defined as the ratio of the residual signal in the data after all backgrounds have been statistically subtracted to the total measured rate, is then determined for each value of y_{cut} and for each jet topology. The values so obtained are given in Table 1 for $z_\gamma > 0.7$ and $z_\gamma > 0.95$ respectively. For example at $y_{cut} = 0.1$ in the 2-jet case, the purity is found to be 0.29 ± 0.03 for $z_\gamma > 0.7$ where 88% of this background arises from π^0s.

Two independent methods are applied to determine the precision of the Monte Carlo simulation for the π^0 production. In the first, it is noted that according to JETSET, at least 90% of inclusively produced π^0s with $z_\gamma > 0.7$ originate from primary quark fragmentation or strong decays of resonances. Hence, in the same kinematic region, isospin invariance can be invoked to equate their rate to the average of inclusive $\pi^\pm$ production. The latter has been determined in ALEPH, with the charged tracks identified as $\pi^\pm$s by dE/dx measurements, for values of $z < 0.8$. The result agrees with JETSET predictions to within 6% between $0.6 < z < 0.8$. Closely similar results have been obtained elsewhere [6]. Thus, since the uncertainties in simulating the efficiency of identifying $\pi^\pm$ are small, the conclusion is that the JETSET generator describes inclusive π^0 production to an accuracy of 6% in this z range.

The second method is less precise statistically but extends over the full range of z up to 1.0. Hard π^0s (and ηs) above 30 GeV are reconstructed from standard hadronic 2-jet events selected over the same range of y_{cut} values. The reconstruction is performed after identifying the conversion of one photon of a pair into e^+e^- in the materials surrounding the interaction region. The candidate V^0s are identified as e^+e^- pairs when their momenta are above 1 GeV, and their masses are confined to be less than 200 MeV. The simulation of such V^0s in the detector agrees closely with those observed both in rate (to 1% up to 20 GeV) and in source radial distribution. Thus, the ratio of selected $e^+e^-\gamma$ combinations (ie those with the smallest opening angle) observed in the data to those from the Monte Carlo represents directly the ratio expected for all π^0 decays in the detector. Fig 3 shows the invariant mass distributions obtained with energies above 30 GeV from the data (609 combinations) and the Monte Carlo (955 combinations) where the π^0 and η peaks are clearly visible on a small background. After fitting these spectra, the ratio of the data to the JETSET prediction is found to be 1.04 ± 0.12 for $z > 0.7$. The distribution of these data in the defined z bins between 0.7 and 0.99 is consistent with JETSET, although in the highest z bin the fractional error is estimated to be as large as $\pm 50\%$. The

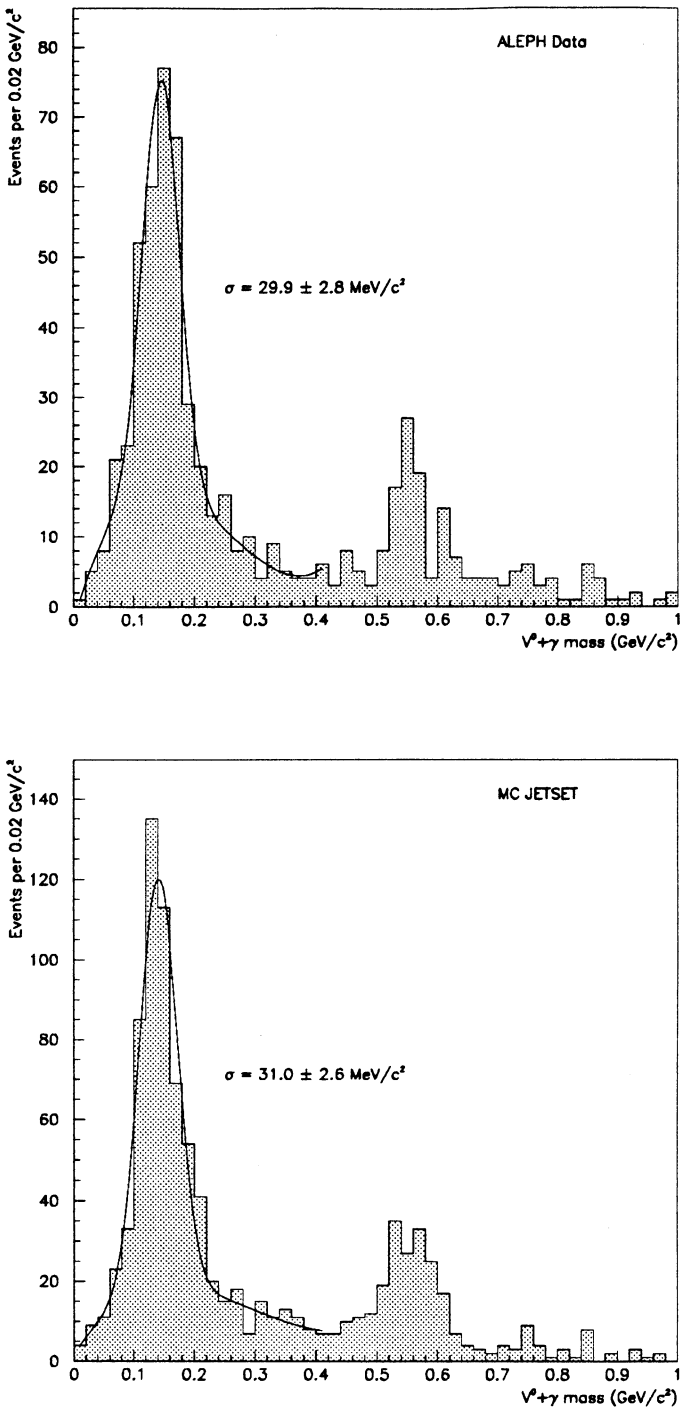

Figure 3: Reconstructed invariant mass distributions for $e^+e^-\gamma$ combinations which have an energy greater than 30 GeV. The π^0 peak is fitted using a Gaussian + a polynomial for the background.

remaining uncertainty is the relative efficiency in reconstructing energetic photon clusters in data and Monte Carlo; this is small compared with the errors quoted above.

These results confirm that JETSET reproduces the overall rate of the observed π^0 background and gives an adequate representation of the differential distribution in z. Taking the uncertainty to be $\pm 6\%$ in the bin $0.7 < z < 0.8$ allows the systematic errors in the z_γ bins defined in Table 2 to determined. These are found to range from $\pm 7.5\%$ to $\pm 55\%$ for bins $0.7 < z_\gamma < 0.75$ to $0.95 < z_\gamma < 0.99$ respectively.

The remaining background of neutral hadrons (ie neutrons, K^0s) misidentified as photons is estimated from the same large Monte Carlo sample above. This background is about 2% for 2-jet topologies below $z_\gamma = 0.9$ independent of y_{cut} and very small for the others.

The final statistical and systematic errors on the corrected n-jet rates are quoted in Table 2. The uncertainties in the z_γ distributions are dominated by statistical errors except for 2-jet events where the systematic and statistical errors are comparable up to $z_\gamma = 0.99$.

3.3 $Z \to \tau^+\tau^-$

This background is estimated by applying the selection on 130 000 fully simulated $Z \to \tau^+\tau^-$ events, generated using KORLO6. It arises from high multiplicity τ decays with an initial state radiation photon or with an isolated photon decaying from a π^0. This background is typically 2–3% of the selected data sample in the 2-jets topology, 0–1% in the 3-jets topology for $0.7 < z_\gamma < 0.99$ and 2% for $z_\gamma > 0.99$. It is however completely negligible in the $\geq$ 4-jet topology.

4 Acceptance Corrections to Hadron Level

In order to compare the data with the QCD matrix element predictions, the measured n-jet rates after subtraction of all backgrounds are corrected for incomplete geometric acceptance, photon conversion losses and reconstruction inefficiencies. These corrections are estimated using a sample of fully reconstructed hadronic events, each containing a prompt photon, generated with a parton shower Monte Carlo and processed with a detailed simulation of the ALEPH detector. A sample of ARIADNE events corresponding to 2.7 million hadronic events is used for this. The results are checked with HERWIG and agree within statistics. No attempt is made to correct the measured jet rates to the parton level i.e. correct for hadronisation effects. Instead, local hadron-parton duality is assumed to apply, namely that the momenta and directions of the observed hadron jets match those of the parton jets formed from the leading hard partons described in the matrix element calculations.

However, the acceptance corrections do include the mixing of event topologies which occur due to detector limitations. The n_i-jet rates at generator level and the resulting n_j-jet rates after the detector simulation and event reconstruction are related by the following equation:

$$\underbrace{(n_j - \text{jets})}_{\text{Detector Level}} = \sum_i \underbrace{(n_i - \text{jets})}_{\text{Generator Level}} \; \mathcal{P}_{i \to j}$$

where the $\mathcal{P}$ matrix elements take into account the efficiency, acceptance and topological mixing effects. The $\mathcal{P}$ matrix elements are computed using the 2.7 million ARIADNE simulated events. Inverting this relation, the inverse matrix, $\mathcal{P}^{-1}$, is then applied to the rates measured in data to deduce the corrected rates. A different matrix $\mathcal{P}^{-1}$ is computed for every z_γ bin at each value of y_{cut}. The statistical uncertainties in the corrected data rates are evaluated by using a simple error propagation of the form:

$$\delta\mathcal{P}^{-1} = \mathcal{P}^{-1}(\delta\mathcal{P})\mathcal{P}^{-1}$$

assuming that each element of $\mathcal{P}^{-1}$ is independent. Table 2 gives the corrected differential rates in z_γ for each jet topology at $y_{cut} = 0.01$ and 0.1.

y_{cut}	All events	2-jet events		3-jet events		$\geq$ 4-jet events	
	photons	photons	FSR purity	photons	FSR purity	photons	FSR purity
0.001	8756	326	$15.8 \pm 6.1\%$	1787	$51.2 \pm 1.7\%$	6643	$57.9 \pm 0.8\%$
0.002	6424	563	$15.5 \pm 4.7\%$	2428	$62.8 \pm 1.2\%$	3433	$67.3 \pm 0.9\%$
0.004	4950	793	$22.1 \pm 3.7\%$	2527	$67.7 \pm 1.1\%$	1630	$73.2 \pm 1.2\%$
0.006	4305	891	$22.1 \pm 3.5\%$	2405	$71.0 \pm 1.0\%$	1009	$76.3 \pm 1.4\%$
0.008	3902	971	$24.0 \pm 3.3\%$	2240	$72.8 \pm 1.0\%$	691	$77.5 \pm 1.7\%$
0.01	3604	1018	$23.8 \pm 3.2\%$	2110	$75.0 \pm 1.0\%$	476	$76.7 \pm 2.0\%$
0.02	2806	1158	$25.6 \pm 3.0\%$	1514	$78.0 \pm 1.1\%$	134	$77.9 \pm 3.7\%$
0.04	2269	1278	$27.3 \pm 2.8\%$	965	$81.2 \pm 1.2\%$	26	$85.8 \pm 6.5\%$
0.06	1988	1321	$27.9 \pm 2.7\%$	661	$81.4 \pm 1.5\%$	6	$79.4 \pm 17.\%$
0.08	1811	1354	$28.6 \pm 2.6\%$	455	$80.6 \pm 1.8\%$	2	$100.0 \pm 0.0\%$
0.1	1710	1375	$28.9 \pm 2.6\%$	335	$82.2 \pm 2.0\%$	0	
0.2	1511	1448	$31.1 \pm 2.5\%$	63	$83.6 \pm 4.5\%$	0	
0.333	1466	1466	$32.0 \pm 2.5\%$	0		0	

y_{cut}	All events	2-jet events		3-jet events		$\geq$ 4-jet events	
	photons	photons	FSR purity	photons	FSR purity	photons	FSR purity
0.001	2613	16	$35.5 \pm 22.5\%$	550	$85.1 \pm 1.4\%$	2047	$87.8 \pm 0.7\%$
0.002	2266	32	$60.0 \pm 11.2\%$	908	$88.5 \pm 0.9\%$	1326	$89.9 \pm 0.7\%$
0.004	1945	48	$62.1 \pm 8.8\%$	1150	$90.6 \pm 0.7\%$	747	$89.6 \pm 1.0\%$
0.006	1730	55	$63.6 \pm 8.0\%$	1192	$91.8 \pm 0.7\%$	483	$90.8 \pm 1.2\%$
0.008	1569	67	$70.1 \pm 6.4\%$	1153	$92.7 \pm 0.6\%$	349	$92.6 \pm 1.2\%$
0.01	1445	73	$69.2 \pm 6.2\%$	1121	$93.6 \pm 0.6\%$	251	$92.1 \pm 1.5\%$
0.02	1082	95	$74.4 \pm 4.8\%$	910	$95.1 \pm 0.6\%$	77	$93.6 \pm 2.4\%$
0.04	768	123	$77.7 \pm 3.9\%$	627	$96.3 \pm 0.6\%$	18	$93.1 \pm 5.1\%$
0.06	589	137	$80.0 \pm 3.4\%$	448	$96.6 \pm 0.7\%$	4	$84.6 \pm 17.\%$
0.08	467	151	$81.8 \pm 3.1\%$	315	$96.0 \pm 0.9\%$	1	$100.0 \pm 0.0\%$
0.1	396	164	$82.9 \pm 2.9\%$	232	$96.4 \pm 1.0\%$	0	
0.2	250	207	$85.6 \pm 2.3\%$	43	$96.1 \pm 2.4\%$	0	
0.333	221	221	$86.5 \pm 2.1\%$	0		0	

Table 1: Number of photons selected in the data sample with (upper) $z_\gamma > 0.7$ and with (lower) $z_\gamma > 0.95$ respectively, and estimated FSR purities in each n-jet class; quoted errors are statistical only.

z_γ bin	2-jet events			3-jet events			$\geq$ 4-jet events		
	Rate	$\pm$ Stat.	$\pm$ Syst.	Rate	$\pm$ Stat.	$\pm$ Syst.	Rate	$\pm$ Stat.	$\pm$ Syst.
0.70–0.75	2.01	$\pm$ 0.82	$\pm$ 0.59	2.32	$\pm$ 0.81	$\pm$ 0.22	0.84	$\pm$ 0.51	$\pm$ 0.03
0.75–0.80	0.77	$\pm$ 0.56	$\pm$ 0.55	2.08	$\pm$ 0.67	$\pm$ 0.18	0.36	$\pm$ 0.35	$\pm$ 0.02
0.80–0.85	0.96	$\pm$ 0.56	$\pm$ 0.51	2.15	$\pm$ 0.67	$\pm$ 0.20	0.91	$\pm$ 0.55	$\pm$ 0.03
0.85–0.90	0.85	$\pm$ 0.48	$\pm$ 0.49	3.49	$\pm$ 0.60	$\pm$ 0.16	0.78	$\pm$ 0.31	$\pm$ 0.01
0.90–0.95	0.64	$\pm$ 0.27	$\pm$ 0.38	4.72	$\pm$ 0.51	$\pm$ 0.13	1.73	$\pm$ 0.37	$\pm$ 0.02
0.95–0.99	0.27	$\pm$ 0.20	$\pm$ 0.21	15.57	$\pm$ 1.11	$\pm$ 0.16	3.50	$\pm$ 0.64	$\pm$ 0.02
0.99–1.00	5.84	$\pm$ 1.60	$\pm$ 0.20	97.32	$\pm$ 5.76	$\pm$ 0.29	21.54	$\pm$ 3.07	$\pm$ 0.11

z_γ bin	2-jet events			3-jet events		
	Rate	$\pm$ Stat.	$\pm$ Syst.	Rate	$\pm$ Stat.	$\pm$ Syst.
0.70–0.75	2.95	$\pm$ 0.80	$\pm$ 0.64	0.25	$\pm$ 0.20	$\pm$ 0.02
0.75–0.80	1.68	$\pm$ 0.62	$\pm$ 0.66	0.00	$\pm$ 0.02	$\pm$ 0.02
0.80–0.85	1.25	$\pm$ 0.53	$\pm$ 0.56	0.09	$\pm$ 0.19	$\pm$ 0.04
0.85–0.90	0.81	$\pm$ 0.42	$\pm$ 0.49	0.50	$\pm$ 0.22	$\pm$ 0.04
0.90–0.95	0.49	$\pm$ 0.23	$\pm$ 0.41	0.56	$\pm$ 0.18	$\pm$ 0.06
0.95–0.99	1.10	$\pm$ 0.28	$\pm$ 0.24	3.28	$\pm$ 0.53	$\pm$ 0.06
0.99–1.00	16.06	$\pm$ 2.49	$\pm$ 0.27	24.48	$\pm$ 3.09	$\pm$ 0.05

Table 2: Rates after background substraction and acceptance corrections measured in the data for (upper) $y_{cut} = 0.01$ and (lower) $y_{cut} = 0.1$ respectively.

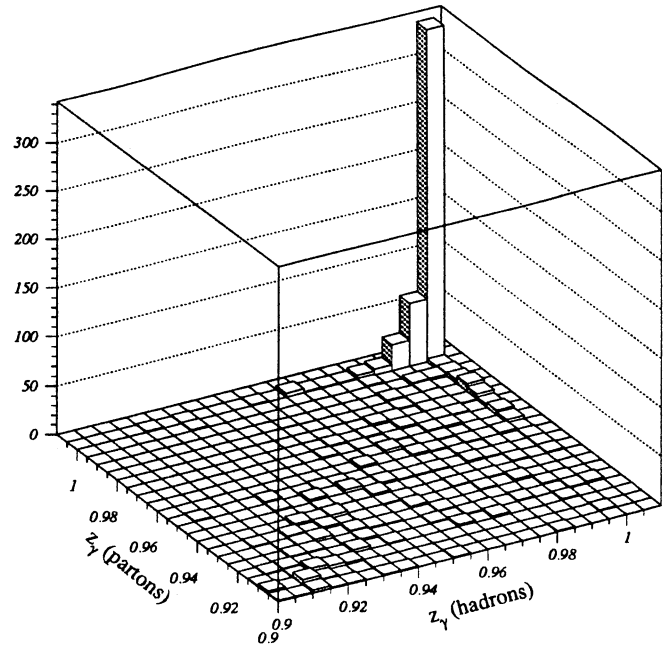

Figure 4: Two-dimensional distributions of z_γ for 2-jet events at parton and hadron level using **ARIADNE** generator ($y_{cut} = 0.1$). The $z_\gamma = 1$ peak in the parton distribution is clearly smeared when the same jets are reconstructed with hadrons.

5 Extraction of the Quark-to-Photon Fragmentation Function and Isolated Photon Components

5.1 2-jet event rates

Between $0.7 < z_\gamma < 0.95$, the corrected differential z_γ distributions show a monotonically decreasing behaviour as expected for values of y_{cut} from 0.01 to the kinematic limit of 0.33. However, there is clear evidence that a fraction (about 20% at $y_{cut} = 0.1$) of the isolated photon component populates the $0.95 < z_\gamma < 0.99$ bin. This effect becomes more pronounced with increasing y_{cut}. Using the **ARIADNE** and **HERWIG** Monte Carlos to study the correlation between the parton and hadron jet reconstruction, it appears qualitatively that this smearing effect is due to the mis-association of soft detected hadrons to the "photon jet" by the recombination algorithm. Fig 4 shows the 2-dimensional distribution obtained using **ARIADNE** of the reconstructed z_γ at parton and hadron levels respectively. The smearing effect occurs at hadron level only. In addition, this effect does not appear to arise from working in the laboratory as the CM frame even in the presence of unobserved initial state radiation. Consequently, the z_γ distributions are analysed in two parts subdivided at $z_\gamma = 0.95$.

5.1.1 Jet Fragmentation region: $0.7 < z_\gamma < 0.95$

This region is used to extract directly the non-perturbative component of the quark fragmentation function, $D_{np}(z_\gamma, \mu_F, \mu_0)$, using the formalism of ref [5]. In this fixed order $\overline{MS}$ renormalisation scheme, it is separated from the calculable perturbative part at a non-physical scale μ_F. The evolution of this non-perturbative component is described analytically so as to cancel the $\ln(1-z_\gamma)^2$ divergences in the perturbative part and remove any overall μ_F dependence in the fragmentation function, $D(z_\gamma)$. It is written as:

$$D_{np} = [A(z_\gamma, \mu_F^2/\mu_0^2) + B(z_\gamma, \mu_0)]/R_{LEP}$$

where A is the prescribed evolution term which together with B specifies the starting value of D_{np}

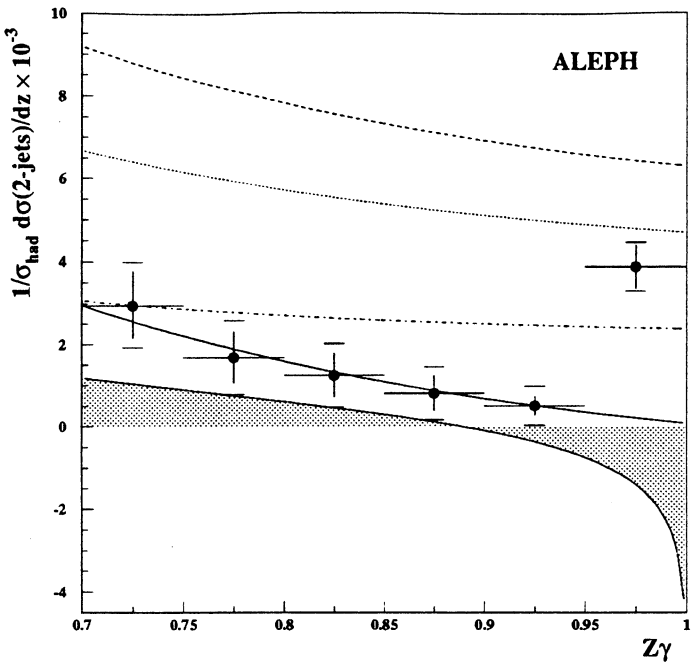

Figure 5: Fit to the quark-to-photon fragmentation region: the shaded area is the perturbative contribution to the fragmentation function ($\mu_F = 10$ GeV). The dashed, dotted and dashed-dotted curves show the addition of the A term to the perturbative contribution for values of μ_0 of 0.2, 1 and 10 GeV respectively.

y_{cut}	fit of C and μ_0			fit with $\mu_0 = 0.2$		fit with $C = -12.5$	
	C	μ_0	$\chi^2/3$	C	$\chi^2/4$	μ_0	$\chi^2/4$
0.008	-13.9 ± 2.8	0.10 ± 0.12	1.48	-12.21 ± 0.39	1.67	0.175 ± 0.028	1.61
0.02	-11.8 ± 3.0	0.24 ± 0.31	0.86	-12.21 ± 0.39	0.87	0.177 ± 0.029	0.89
0.06	-12.4 ± 3.0	0.20 ± 0.25	0.31	-12.38 ± 0.36	0.31	0.190 ± 0.030	0.31
0.1	-12.9 ± 2.9	0.16 ± 0.20	0.35	-12.45 ± 0.35	0.37	0.195 ± 0.029	0.37
0.33	-12.9 ± 2.7	0.16 ± 0.18	0.68	-12.31 ± 0.35	0.71	0.184 ± 0.028	0.69

Table 3: Results of fitting the non-perturbative part D_{np} of the quark-to-photon fragmentation function.

when $\mu_F = \mu_0$. At the Z, R_{LEP} is the ratio of the hadronic to the inclusive FSR cross section and takes the value 3.98×10^3 [5].

Various parametrisations of B have been tried in fitting $D(z_\gamma)$ to the five data points in z_γ for y_{cut} values of 0.008,0.02,0.06, 0.1 and 0.33. These included a form :

$$B(z_\gamma, \mu_0) = C\ (1 + z_\gamma)^\beta$$

in which the free parameters are μ_0, C and β. The data do not support simultaneous exploration of this 3-dimensional parameter space, but it is found that good fits are obtained with $\beta = 0$. (ie no z_γ dependence is required). This behaviour is illustrated in Fig 5 which shows a fit obtained in the jet fragmentation region at $y_{cut} = 0.1$. This is a 2 parameter fit from which values of C and μ_0 are found to be:

$$\begin{cases} C &= -12.9 \pm 2.9 \\ \mu_0 &= 0.16 \pm 0.20\ GeV \end{cases}$$

Thus, a low value of the initial evolution scale is preferred, and a constant off-set must be *subtracted* from the evolution term to match the data. The data do not support a zero off-set for any value of μ_0. The fitted $D(z_\gamma)$ function also extrapolates to zero at $z_\gamma = 1$ as expected. Table 3 shows all the results obtained from double and single parameter fits to the z_γ distributions at the 5 y_{cut} values above. The errors in the double parameter fit are strongly correlated, which leads to smaller errors when the single parameter fits are performed. Consistent values for C and μ_0 are found showing that over this range of y_{cut}, the D_{np} function is universal as expected in this formalism, and any y_{cut} dependence in $D(z_\gamma)$ is taken care of by the perturbative part.

Fig 6 shows the comparison, for four different values of y_{cut}, between the fully measured z_γ distributions and an analytical calculation of the predicted rates coming from a combination of the fitted $D(z_\gamma)$ function and the isolated photon component at $z_\gamma = 1$ [5]. For this purpose, the values of C and μ_0 found at $y_{cut} = 0.06$ are chosen to describe the universal behaviour of the non-perturbative component.

5.1.2 Isolated photon region: $0.95 < z_\gamma < 1$

The discrepancy in the $0.95 < z_\gamma < 0.99$ range between the corrected rate and the $D(z_\gamma)$ function is now very clear (Fig 6), but it is interesting to note that there is very good agreement between the calculated isolated component and the data in the highest z_γ bin alone. However, as described previously studies indicate that the discrepancy is due to smearing of the isolated component by particle mis-association. Hence, the integrated rates above $z_\gamma = 0.95$ are compared with the combined prediction which includes the fragmentation contribution. Fig 7 shows the result of this comparison as a function of y_{cut}. Overall, the agreement is good even below $y_{cut} = 0.01$ where this fixed order calculation is not expected to be valid. The 20% discrepancy at high y_{cut} may be accounted for by higher order corrections [7]. In contrast to ARIADNE and HERWIG predictions which compare well with the data, Fig 7 shows that JETSET falls well below the data in this region of phase space. It should be noted that in the "democratic" approach the isolated photon rate at this order of calculation depends only on y_{cut} and the Z electro-weak couplings, and not α_S.

5.2 3- and $\geq$4-jet event rates

As shown in Fig 2, the z_γ distributions for 3- and $\geq$4-jet events display relatively small fragmentation contributions and non-prompt hadronic backgrounds compared with those observed for the 2-jet case. For 3-jet events, this is not unexpected since the quark fragmentation function now appears at next-to-leading order, and the gluon fragmentation function, which appears at lowest order, is expected to be small when $z_\gamma > 0.7$. These fragmentation processes are suppressed by a further order of α_S in the 4-jet case and hence are not calculated in the following QCD predictions.

The corrected z_γ distributions are compared at each value of y_{cut} with the full $\mathcal{O}(\alpha\alpha_S)$ calculation [5] which now includes the non-perturbative part of the $D(z_\gamma)$ quark fragmentation function measured

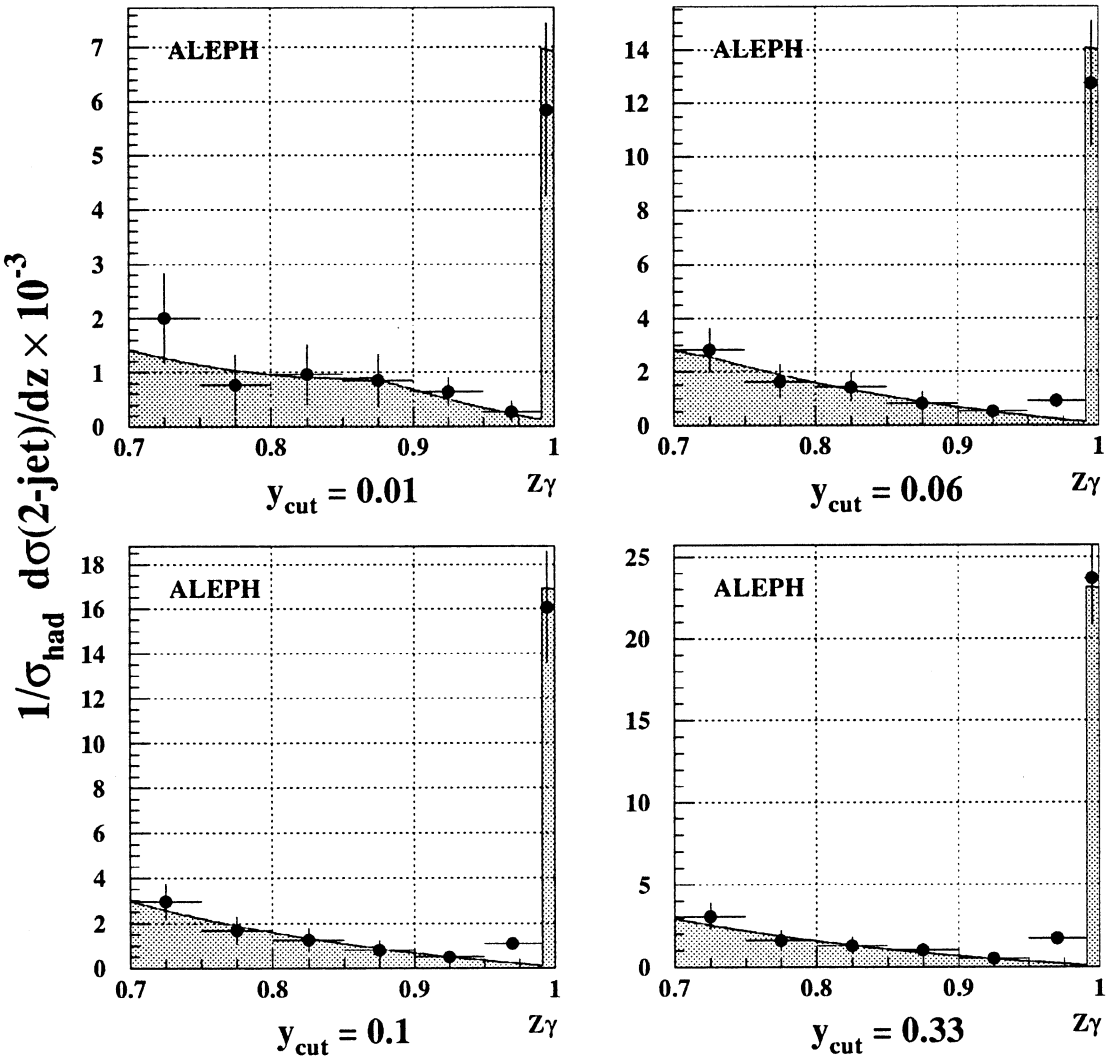

Figure 6: Comparison between the 2-jet rates measured for 4 different values of y_{cut} and the analytical calculation including the universal fitted non-perturbative component of the quark-to-photon fragmentation function.

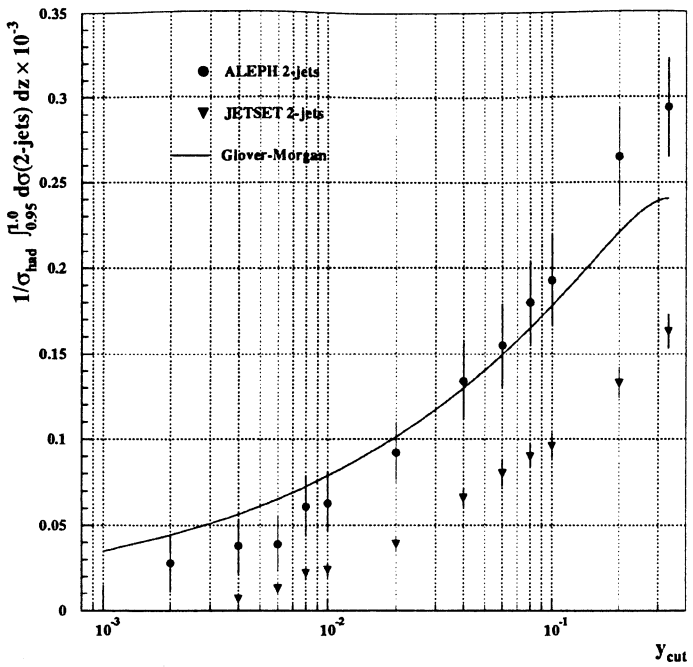

Figure 7: Integrated 2-jet rate above $z_\gamma = 0.95$ as function of y_{cut}, compared with the full QCD calculation including the fitted non-perturbative component of the $D(z_\gamma)$ function.

from the 2-jet rate. Thus, it is expected that the calculated rates will depend only on α_S and not on the choice of the fragmentation scale μ_F. This treatment is implemented in an updated Monte Carlo program EEPRAD [2] which includes the fragmentation processes and allows the experimental photon energy cut at 5 GeV to be implemented. Fig 8 show the comparison between the corrected data and EEPRAD at $y_{cut} = 0.01, 0.04$ respectively. With $\alpha_S = 0.12$ [8] and the gluon fragmentation contribution ignored, the $0.7 < z_\gamma < 0.9$ fragmentation region is well described by EEPRAD. However, at higher z_γ there is strong evidence that part of the isolated photon component in the data is smeared from $z_\gamma = 1$ by mis-association of reconstructed hadrons to the "photon" jet. In this case, the effect is more pronounced than observed for the 2-jet events, but again the parton shower models confirm qualitatively that the origin of the effect is the difference between parton and hadron clustering to the FSR photon in the DURHAM algorithm. Thus, the *integrated* rates above $z_\gamma = 0.9$ are compared with EEPRAD over a wide range of y_{cut}, with no attempt being made to separate the isolated photon component (R_Δ) from the underlying fragmentation function. In any case, the $q\bar{q}\gamma g$ matrix element contributes to both R_Δ and the parton fragmentation functions, so in principle R_Δ cannot be isolated. Fig 9 shows that with $\alpha_S = 0.12$, the EEPRAD integrated 3-jet prediction follows the data to within statistical errors ($\leq 6\%$) at high y_{cut} where the 4-jet rate is not significant. At lower values of y_{cut}, the discrepancy becomes very large but can be eliminated simultaneously in both the 3-jet and $\geq$ 4-jet rates, down to y_{cut} values of ~ 0.004, by increasing α_S empirically to 0.17. Effectively, this choice of α_S in such a NLO calculation is compensating for the missing higher orders and other scheme dependent factors [9]. However, it may be interesting to note that where the 4-jet rate is negligible, the all-orders value of 0.12 gives better agreement with the data. It is also found that the 3-jet fragmentation region, as illustrated in Fig 8, is better described by this choice of $\alpha_S = 0.12$ even at values of y_{cut} where it is no longer valid elsewhere.

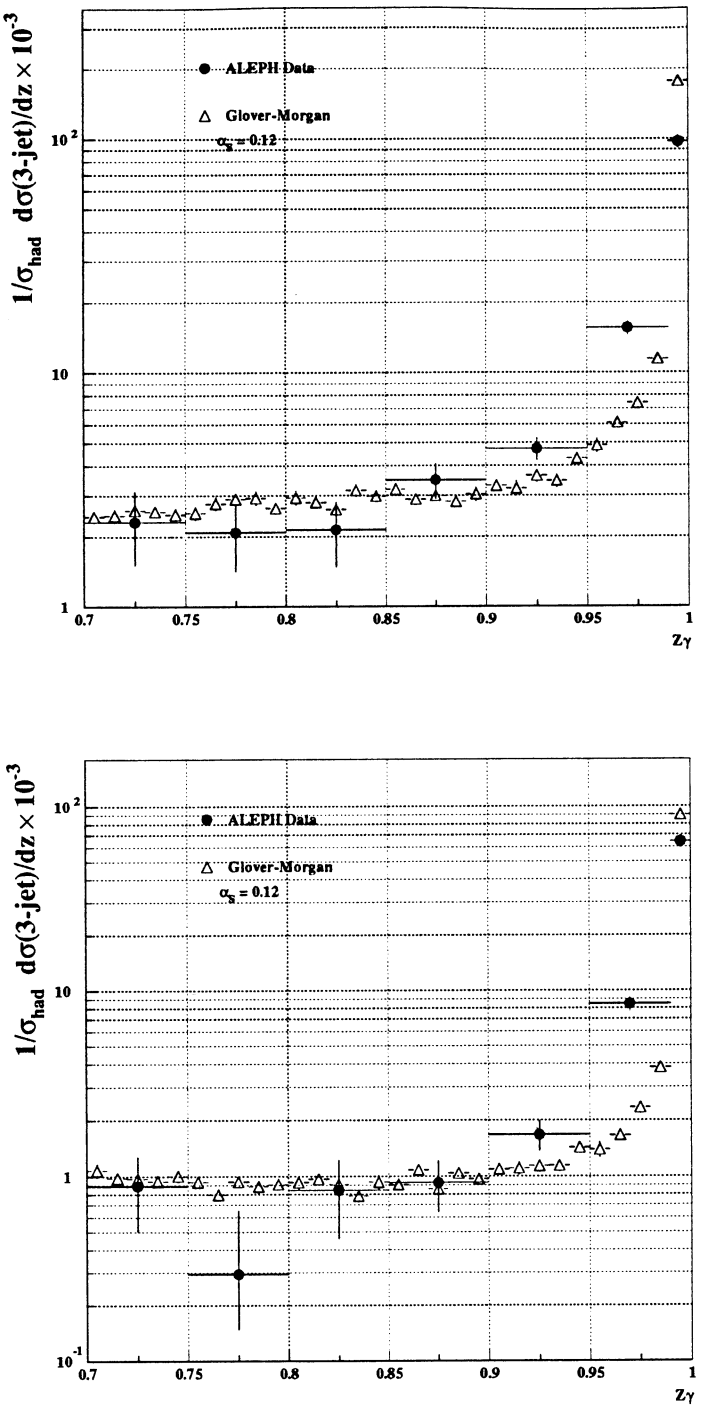

Figure 8: The 3-jet differential rates for (upper) $y_{cut} = 0.01$ and (lower) $y_{cut} = 0.04$ compared with the $\mathcal{O}(\alpha\alpha_S)$ calculation which includes the non-perturbative part of the $D(z_\gamma)$ fragmentation function measured from the 2-jet rate.

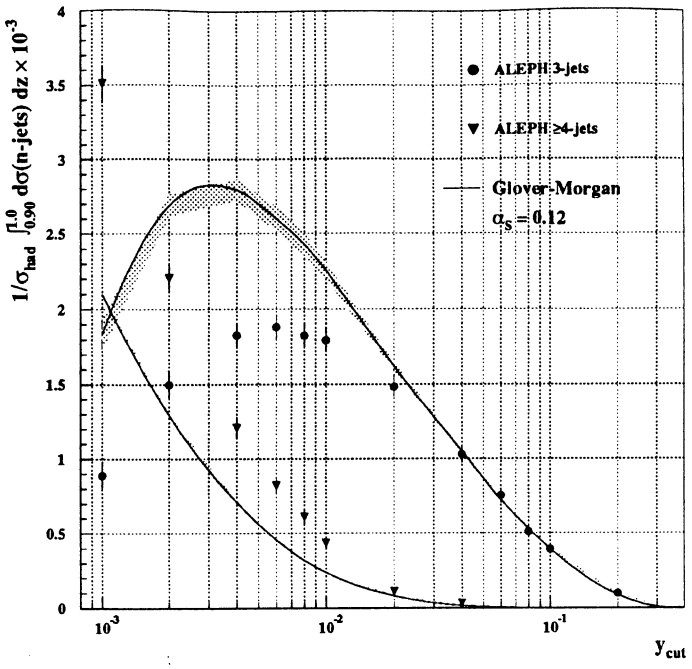

Figure 9: The 3-jet and $\geq$ 4-jet integrated rates with $z_\gamma \geq 0.90$ as a function of y_{cut}, compared with EEPRAD predictions (solid lines).

5.3 Integrated z_γ rates

Further comparisons between the n-jet rates integrated from a z_γ threshold, z_{cut}, and the predictions of ARIADNE and JETSET are shown in Fig 10 for $y_{cut} = 0.01$. They demonstrate that even though ARIADNE agrees closely with the data when $z_{cut} > 0.99$ for all jet topologies, it tends to rise above the data as z_{cut} is reduced. Conversely, JETSET matches the shape of the measured z_{cut} distributions well but shows a constant offset which originates in its failure to describe the isolated component satisfactorily at $z_\gamma = 1$.

6 Conclusions

Using the DURHAM jet finding algorithm in a "democratic" event analysis, we have measured the high z part of the quark-to-photon fragmentation function for the combination of quarks decaying from the Z resonance peak at LEP. We have extracted the non-perturbative part of this function within a fixed order $\overline{MS}$ renormalisation scheme and shown that when its contribution is taken into account, an excellent description of all aspects of the measured n-jet rates can be found.

Acknowledgements

We wish to thank Nigel Glover and Andrew Morgan for many useful discussions.

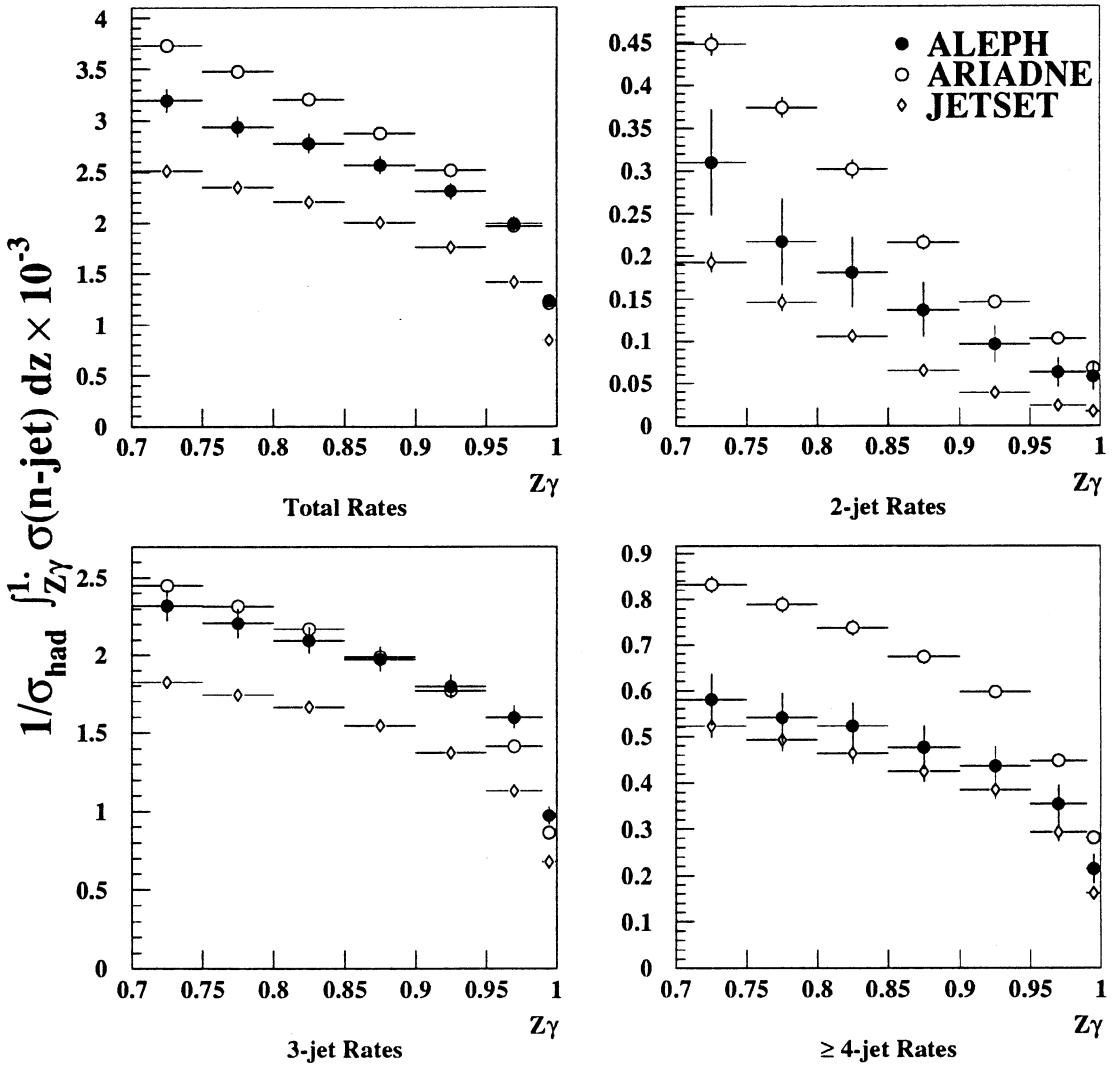

Figure 10: Integrated n-jet rates as a function of the z_{cut} at for $y_{cut} = 0.01$, compared with the predictions of ARIADNE and JETSET.

References

[1] OPAL Collaboration, P.D. Acton et al., *Z Phys.* **C58** (1993) 405,
ALEPH Collaboration, D. Buskulic et al., *Z Phys.* **C57** (1993) 17,
DELPHI Collaboration, P. Abreu et al., *Z Phys.* **C53** (1992) 555,
L3 Collaboration, O. Adriani et al., *Phys. Lett.* **B292** (1992) 472.

[2] E.W.N.Glover and W.J.Stirling, *Phys. Lett.* **B295** (1992) 128.

[3] G.Kramer and H.Spiesberger, DESY 92-022 (1992).

[4] P. Mättig, H. Spiesberger and W. Zeuner, *Z Phys.* **C60** (1993) 613.

[5] E.W.N.Glover and A.G.Morgan, DTP/93/50, to appear in *Z Phys.* **C**.

[6] OPAL Collaboration, P.D. Acton et al., CERN-PPE/94-49.

[7] E.W.N.Glover and A.G.Morgan, *Phys. Lett.* **B324** (1994) 487.

[8] The LEP Collaborations and the LEP Electroweak Working Group, CERN/PPE/93-157.

[9] D.T. Barclay, C.J. Maxwell and M.T. Reader, DTP/93/68.